communications biology

A Nature Portfolio journal

Article

https://doi.org/10.1038/s42003-025-09182-6

Dual-action salivary peptide drives black fly feeding efficiency

Xiaopei Yang[1,3], Yanmei He[1,3], Xiaoli Feng[1,3], Guixi Wang[1], Xiaoyan Zhou[1], Lixian Mu[1,4] ✉, Jing Wu[1,4] ✉ & Hailong Yang[1,2,4] ✉

Black flies (Simulidae) employ salivary peptides to optimize blood-feeding efficiency through anticoagulation and analgesia, yet the molecular mechanisms underlying their analgesic effects remain unclear. Here, we identified a novel Kunitz-type peptide, sibanin, from *Simulium bannaense* venom, which exhibits both potent analgesic and anticoagulant properties. Using pain activity tracking, HPLC, and electrophysiological techniques, we found that sibanin potently inhibited the $Na_V1.7$ channel (IC_{50}: 265.03 ± 7.86 nM), selectively reducing pain signal transmission in mouse thermal pain models. Mutagenesis studies identified critical residues (N209 and A1585) in the $Na_V1.7$ voltage-sensing domain (S3b-S4a) essential for sibanin binding, conserved across vertebrate hosts. Concurrently, sibanin inhibited coagulation factors (e.g., FXa) and proteases, preventing thrombus formation. This dual functionality enables black flies to suppress host pain perception and ensure continuous blood flow during feeding. The unique synergy of $Na_V1.7$-targeted analgesia and anticoagulation highlights sibanin's potential as a lead compound for dual-action therapeutics in pain management and thrombotic disease treatment, circumventing polypharmacy risks. Our findings elucidate a conserved evolutionary strategy in hematophagous insects and provide a foundation for developing multifunctional pharmacological agents.

In the complex and competitive natural environment, animals have evolved a diverse array of strategies to enhance their survival, whether through hunting prey or defending against predators. One notable adaptation is the use of toxins, which has been perfected by several species to optimize their survival capabilities. For example, Centipede, as an ancient carnivorous poisonous animal, contains many bioactive components in its venom, which enables the centipede to swiftly incapacitate prey that may weigh more than 15 times its own body weight within just 30 s[1]. Similarly, scorpions employ neurotoxins in their venom for defense, deterring predators by inducing intense pain. Research has elucidated that peptide toxins within scorpion venom can specifically activate the capsaicin receptor (TRPV1), triggering a rapid and severe pain response[2]. By enhancing their predatory efficiency or defensive capabilities of certain animals, these species are better equipped to thrive in their respective ecological niches.

Blood-sucking animals have significantly optimized their survival adaptability by evolving complex toxin systems. These animals mainly include vampire bats, ticks, mosquitoes, and leeches. Their saliva or venom contains many bioactive substances, which play a key role in the process of preying on and spreading pathogens. The saliva of vampire bats contains a variety of anticoagulant and analgesic substances, which can effectively prevent blood coagulation and reduce the pain response of the host, thus optimizing its blood-sucking process[3,4]. The salivary gland of *Aedes aegypti* contains immunosuppressive toxin proteins (such as LTRIN), which can reduce the immune level of blood-sucking parts by inhibiting the host's lymphotoxin β receptor signaling pathway, thus assisting the spread of pathogens such as the Zika virus. This immunosuppressive mechanism not only optimizes the blood-sucking process of *A. aegypti*, but also enhances its ability as a vector-borne pathogen[5]. The saliva of leeches contains a variety of anticoagulant and analgesic substances, which can effectively prevent blood coagulation and alleviate the pain response of the host, thus optimizing its blood-sucking process[6,7]. In addition, the genome study of the leech also found that the gene family expansion of the leech is mainly concentrated in the functional pathways related to calcium ion binding and ATP transport, and the expansion of these genes may be closely related to its blood-sucking habits[8].

Black flies (Simuliidae) belong to the family Simuliidae within the order Diptera and are important hematophagous insects. In the family Simuliidae, approximately 90% of the species require blood feeding by females to

[1]School of Basic Medical Sciences, Kunming Medical University, Kunming, China. [2]Yunnan Key Laboratory of Stem Cell and Regenerative Medicine, School of Rehabilitation, Kunming Medical University, Kunming, China. [3]These authors contributed equally: Xiaopei Yang, Yanmei He, Xiaoli Feng.[4]These authors jointly supervised this work: Lixian Mu, Jing Wu, Hailong Yang. ✉e-mail: mulixian77@163.com; wujing_205@163.com; jxauyhl@163.com

promote egg maturation[9]. During blood-feeding, the saliva of black flies contains a diverse array of peptides that play crucial roles in anticoagulation, antimicrobial activity, and immune regulation[10]. For example, studies on the salivary proteome of the black fly *Simulium vittatum* have revealed that its saliva contains multiple proteins associated with blood feeding[11]. Further investigations have revealed that a salivary gland protein named Simukunin can inhibit blood coagulation and inflammatory responses, thereby helping black flies evade host defense mechanisms during blood-feeding[12]. Recent studies have also uncovered a novel Kunitz-type protease inhibitor, sibanin, purified from the salivary glands of the Banna black fly (*Simulium bannaense*)[13]. Sibanin exhibits significant anticoagulant and anti-platelet aggregation properties by inhibiting blood coagulation and platelet aggregation, effectively preventing thrombus formation[13]. The discovery of this peptide not only enhances our understanding of the functional diversity of black fly salivary peptides but also provides a potential candidate for the development of novel anticoagulant drugs.

While the mechanisms by which black flies (Simuliidae) employ toxins to enhance their blood-feeding efficiency have been well-documented, the specific mechanisms underlying their potent analgesic effects remain largely unexplored. In this study, we employed a combination of pain activity tracking, high-performance liquid chromatography (HPLC), and patch-clamp electrophysiological techniques to screen the crude venom of *S. bannaense*. Our findings revealed that sibanin, a novel Kunitz protease inhibitor, exhibits both anticoagulant and analgesic activities. In animal models, sibanin showed remarkable analgesic activity in a mouse thermal pain model. Furthermore, sibanin efficiently inhibited the excitability of DRG neurons. Target screening results indicated that sibanin selectively inhibits the $Na_V1.7$ channel with high specificity. Further investigations elucidated the interaction mechanisms between sibanin and the $Na_V1.7$ channel and identified the key amino acid residues targeted by sibanin on $Na_V1.7$. Interestingly, these key amino acid residues are highly conserved among the host species of black flies. Given that sibanin possesses both significant anticoagulant activity and potent analgesic effects, these results suggest that black flies may utilize sibanin to simultaneously exert analgesic and anticoagulant actions during blood feeding, thereby facilitating more efficient blood acquisition.

Results

Isolation and identification of analgesic components from black fly venom

Black flies employ salivary components to enhance blood-feeding efficiency (Fig. 1a). Following microdissection of *S. bannaense* salivary glands, we isolated components exhibiting analgesic effects using peptide purification coupled with analgesic bioassays, integrating with thermal and mechanical nociception assays (Fig. 1b, c and Supplementary Fig. 1a). This approach led to the identification of a small peptide toxin (GenBank MK689374) with a molecular weight of 10,557.3 Da (Fig. 1d). Through combined Edman sequencing and cDNA library screening, we resolved the complete 110-residue precursor architecture, revealing proteolytic processing that excises a 19-residue signal peptide to generate the 91-amino acid mature toxin (Supplementary Fig. 1b). BLAST analysis of the mature peptide's primary sequence revealed similarity to the known animal toxin sibanin. Structural characterization using AlphaFold2 AI-powered modeling platform unveiled a conserved Kunitz-type fold stabilized by three distinctive disulfide connectivities (Cys6-Cys56, Cys15-Cys39, and Cys31-Cys52) and a cationic C-terminal domain (Fig. 1e, f). The structure of sibanin is stable through three disulfide bond connection modes, a typical Kunitz domain, and a highly basic C-terminal (Fig. 1f).

Sibanin demonstrates potent analgesic activity on pain models

Following the identification of sibanin from the venom of *S. bannaense*, we investigated its analgesic effects using heat-induced and paclitaxel-induced

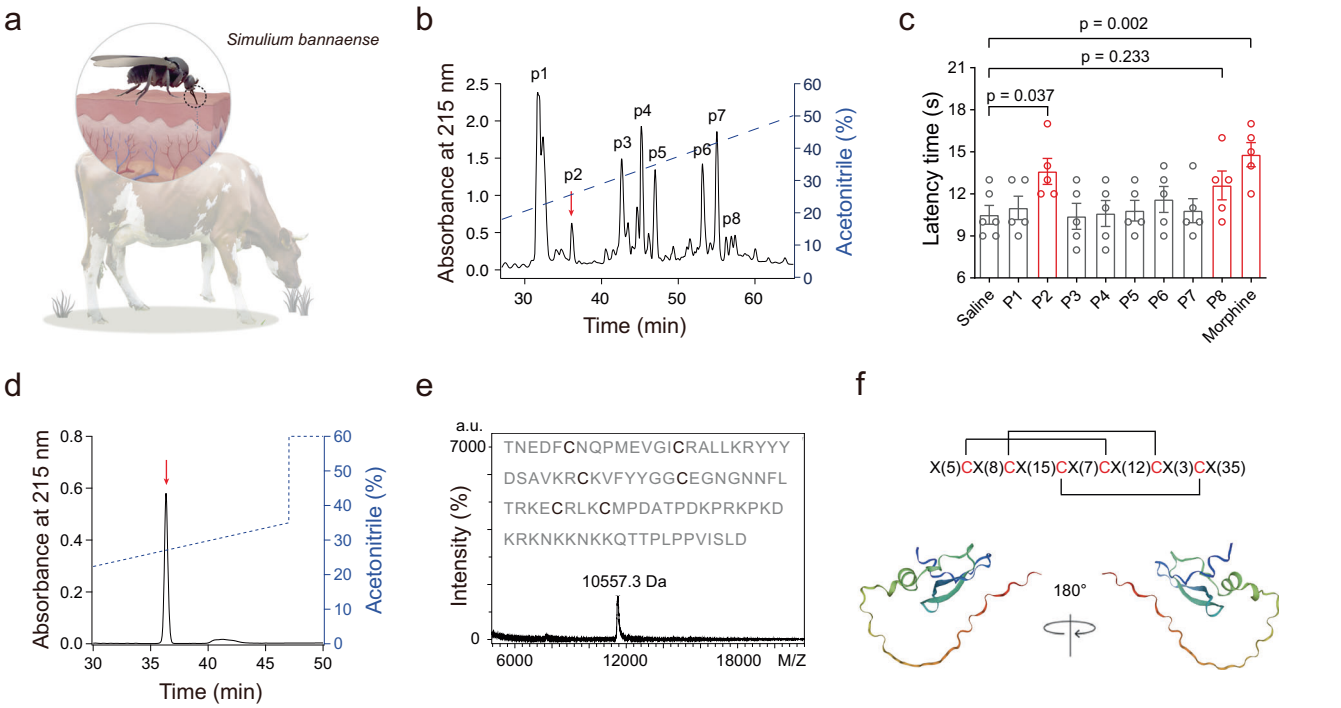

Fig. 1 | Purification and structural characterization of sibanin peptide from *S. bannaense*. **a** Schematic diagram of *S. bannaense* (black fly) feeding on bovine blood. **b** Isolation of native sibanin (red arrow) from the crude salivary gland of *S. bannaense* by a C_{18} RP-HPLC column. Reverse-phase HPLC chromatogram of sibanin purification. Absorbance at 215 nm (a.u.) is plotted against elution time (min), with the arrow indicating the peak corresponding to sibanin. **c** Summary of the analgesic efficacy against heat-induced pain after intraperitoneal administration of *S. bannaense* salivary-gland components compared to morphine (0.2 mg/kg). One-way ANOVA with Bonferroni post-hoc correction. $n = 5–6$ for each peak. **d** Isolation of native sibanin (red arrow) from the pooled protein fraction by a C_{18} RP-HPLC column. **e** MALDI-TOF mass spectrometry confirms the molecular weight of sibanin (10,557.3 Da). **f** Schematic representation of sibanin's cysteine framework and sequence motifs. pLDDT = 82.8. pTM = 0.602.

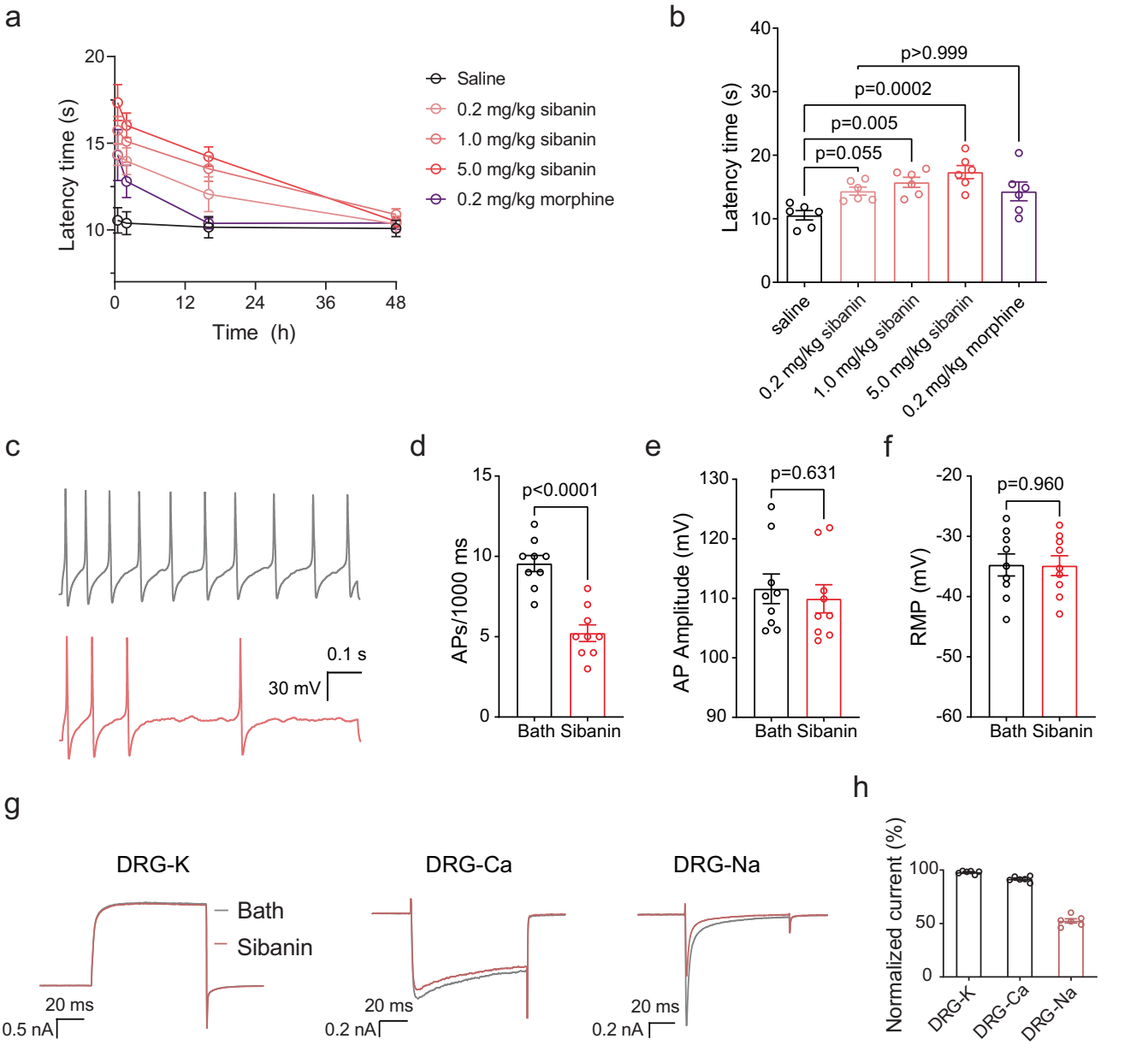

Fig. 2 | Sibanin attenuates pain behavior and modulates action potential properties in dorsal root ganglion (DRG) neurons. a Time course of pain behavioral latency in mice treated with saline (control), Sibanin (0.2, 1.0, 5.0 mg/kg), or morphine (0.2 mg/kg). Latency time (s) was measured at 30, 120 min, 16 h, and 48 h post-injection. $n = 6$. **b** Dose-dependent analgesic efficacy of sibanin vs morphine control 30 min post-intraperitoneal administration. One-way ANOVA with *Bonferroni* post-hoc correction. $n = 6$. **c** Representative action potential (AP) traces from DRG neurons depict the baseline activity (top) and the response recorded after the application of sibanin (bottom), which was administered following the establishment of stable AP recordings. Scale bars: 0.1 s (horizontal), 15 mV (vertical). Current-clamp recording shows that 200 nM sibanin decreases the excitability of small DRG neurons from WT mice. Bars show significant changes for AP spike number (**d**, $n = 9$, parametric paired two-tailed *t* test), but no effect on AP amplitude (**e**, $n = 9$, parametric paired two-tailed *t* test) and resting membrane potential (RMP) (**f**, $n = 9$, parametric paired two-tailed *t* test) in the presence of 200 nM sibanin. **g** Representative whole-cell currents mediated by voltage-gated K^+ (DRG-K), Ca^{2+} (DRG-Ca), and Na^+ (DRG-Na) channels in rat DRG neurons before (black) and after (red) application of sibanin. **h** Summary of the normalized peak currents for each channel type in the presence of sibanin ($n = 6$ cells per group).

neuropathic pain models. Notably, isolated sibanin proved insufficient for molecular/animal studies; therefore, subsequent experiments used heterologously expressed protein. The analgesic experimental design incorporated: vehicle control (isotonic saline, 100 µL via intraperitoneal administration), opioid analgesic comparator (morphine hydrochloride, 0.2 mg/kg intraperitoneal injection), and test peptide (0.2, 1.0, and 5.0 mg/kg sibanin administered via intraperitoneal route). To account for pharmacokinetic parameters, test substance administration preceded behavioral testing by 30 min—a time window validated through preliminary absorption studies to achieve peak plasma concentrations. In the hot plate test, pretreatment with sibanin significantly increased the latency time. Intraperitoneal injections of sibanin showed a dose-dependent and time-dependent increase in latency time (Fig. 2a, b). Specifically, sibanin increased the latency time by 22.86%, 37.14%, and 50.00% at concentrations of 0.2, 1.0, and 5.0 mg/kg, respectively, 30 min after administration. Notably, 0.2 mg/kg of sibanin exhibited analgesic activity comparable to that of morphine at the same mass concentration, suggesting that sibanin possesses potent analgesic efficacy against heat-induced pain. Consistent with these findings, sibanin administration (0.2-5.0 mg/kg, i.p.) dose-dependently reversed paclitaxel-induced reductions in mechanical nociceptive

thresholds in a neuropathic pain model, as measured by the von Frey filament test (Supplementary Fig. 2).

Sibanin-mediated attenuation of nociceptor excitability

As primary transducers of nociceptive signaling, small-diameter (< 30 μm) DRG neurons (nociceptors) constitute the initial relay station for peripheral pain transduction[14]. Employing whole-cell patch-clamp electrophysiology in murine nociceptors, we systematically quantified sibanin's neuromodulatory effects on neuronal excitability. Current-clamp recordings revealed that 200 nM sibanin significantly inhibited neuronal firing frequency in DRG neurons, exhibiting 44.53 ± 5.66% suppression of action potential discharge rates (Fig. 2c, d, $p < 0.01$ vs bath). Notably, this inhibition occurred without altering fundamental biophysical parameters: resting membrane potential, baseline = −34.75 ± 1.84 mV vs sibanin = −34.88 ± 1.65 mV ($n = 9$, $p = 0.96$, paired t-test); action potential amplitude: baseline = 111.60 ± 2.50 mV vs sibanin = 109.92 ± 2.37 mV ($n = 9$, $p = 0.63$, paired t-test). This selective inhibition pattern (Fig. 2e, f) suggests a mechanism distinct from generalized membrane stabilization, potentially involving state-dependent modulation of voltage-gated ion channels rather than passive membrane property alterations.

Electrophysiological effects of sibanin on DRG neurons

Given the pivotal role of voltage-gated ion channels in the transmission of action potentials to the spinal cord, we employed whole-cell electrophysiological techniques to assess the effects of sibanin on voltage-gated sodium (Na_V), potassium (K_V), and calcium channels (Ca_V) expressed in DRG neurons (Fig. 2g). As illustrated in Fig. 2g, 200 nM sibanin had no effect on K_V channels in DRG neurons. It exhibited minimal inhibition (~10%) of Ca_V channels in DRG, but a marked inhibitory effect (~45%) on Na_V channels in DRG was observed (Fig. 2h). These observations suggest that sibanin might exert its potent analgesic effects by selectively targeting voltage-gated sodium channels.

Sibanin potently inhibits the $Na_V1.7$ channel

Capitalizing on the established pathophysiological significance of $Na_V1.7$, $Na_V1.8$, and $Na_V1.9$ channels in nociceptive transduction within DRG neurons[15,16], these channels have emerged as promising targets for pain modulation. To elucidate the specific sodium channel subtype targeted by sibanin, we conducted whole-cell patch-clamp recordings in human embryonic kidney (HEK) 293T cells heterologously expressing $Na_V1.7$, $Na_V1.8$, and $Na_V1.9$ channels. Our results demonstrated that sibanin selectively inhibited the $Na_V1.7$ (SCN9A-encoded) channel, with no significant effects on $Na_V1.8$ (SCN10A-encoded) or $Na_V1.9$ (SCN11A-encoded) channels (Fig. 3a and supplementary Fig. 3). Specifically, in the presence of 200 nM sibanin, the peak current amplitude of $Na_V1.7$ was significantly reduced, whereas the currents through $Na_V1.8$ and $Na_V1.9$ remained largely unaffected. Consistently, we observed a progressive reduction in $Na_V1.7$ current amplitude with increasing concentrations of sibanin (Fig. 3b, inset). The half-maximal inhibitory concentration (IC_{50}) of sibanin for $Na_V1.7$ was determined to be 265.03 ± 7.86 nM (Fig. 3b).

High selectivity of sibanin on $Na_V1.7$ channel

To further investigate the specificity of sibanin, we tested its effects on other ion channels commonly expressed in sensory neurons, including $K_V1.3$, $K_V2.1$, $Ca_V2.2$, TRPV1, TRPV2, TRPV3, TRPV4, and TRPA1. Our results indicated that 200 nM sibanin did not significantly alter the currents through these channels (Fig. 3c–k). Voltage-gated ion channels such as $K_V1.3$, $K_V2.1$, and $Ca_V2.2$ channels have been reported to play a role in pain sensation[17–19]. Application of 200 nM sibanin on these channels had no remarkable activity (Fig. 2f–h). TRP channels, including TRPV1, TRPV2, TRPV3, TRPV3, TRPA1 and TRPM8 channels, have been reported to be involved in pain signaling[20–22], and the currents of these channels were recorded by a voltage ramp from −100 mV to +100 mV for 500 ms. the application of 200 nM sibanin did not affect the currents evoked by 1 μM capsaicin (TRPV1) or 500 μM 2-APB (TRPA1), suggesting that sibanin selectively targets $Na_V1.7$ without affecting other ion channels involved in sensory signaling.

Modulation of $Na_V1.7$ channel dynamics by sibanin

To further elucidate the effects of sibanin on $Na_V1.7$ channel properties, we investigated changes in $Na_V1.7$ channel kinetics before and after drug application, focusing on voltage-dependent activation and inactivation, recovery from inactivation, and use-dependence. Cells were held at −120 mV and subjected to a series of depolarizing pulses ranging from −80 mV to +30 mV in 10-mV increments for 50 ms to construct the voltage-dependent activation curve of $Na_V1.7$ (Fig. 4a). In the presence of 200 nM sibanin, the peak current of $Na_V1.7$ was reduced by approximately 46% (Fig. 4b). Additionally, the voltage dependence of activation was significantly shifted to the left, with the half-activation voltage (V_{50}) changing from −0.78 ± 2.29 mV to −11.56 ± 2.12 mV (Fig. 4c). This indicates that 200 nM sibanin significantly affects $Na_V1.7$ activation by shifting the activation curve towards more hyperpolarized potentials. The steady-state inactivation of $Na_V1.7$ was examined by holding cells at −120 mV and applying 1-s pre-pulses ranging from −140 mV to +20 mV in 10-mV increments, followed by a test pulse to −20 mV for 20 ms to assess channel availability (Fig. 4d). In the presence of 200 nM sibanin, the steady-state inactivation curve of $Na_V1.7$ was shifted to the left by 12.55 mV, with the half-inactivation voltage (V_{50}) changing from −44.55 ± 2.76 mV to −57.10 ± 2.89 mV. This suggests that sibanin enhances the inactivation of $Na_V1.7$ channels.

The recovery time constant from inactivation reflects the affinity of the compound for the inactivated state of the channel. Cells were held at −120 mV and depolarized to −10 mV for 50 ms, with varying intervals at −120 mV between pulses to allow recovery from inactivation. The normalized current of the second pulse relative to the first pulse was plotted against the recovery time, and the recovery time constant was obtained by fitting the data with a single exponential equation (Fig. 4e). In the presence of 200 nM sibanin, the recovery time constant from inactivation was significantly prolonged from 2.50 ± 0.16 ms to 5.66 ± 0.18 ms, indicating that 200 nM sibanin delays the recovery of $Na_V1.7$ channels from inactivation. To investigate whether the inhibitory effect of sibanin on $Na_V1.7$ is use-dependent, cells were subjected to a train of 20-ms depolarizing pulses to 10 mV at a frequency of 10 Hz (Fig. 4f). In the absence of sibanin, the control group exhibited no significant current rundown, with the current amplitude remaining above 95% of the initial value. However, after 1 min of incubation with 200 nM sibanin, a significant reduction in current amplitude was observed under 10 Hz stimulation (Fig. 4f). This suggests that the blockade of $Na_V1.7$ by sibanin is use-dependent.

Direct interaction between sibanin and $Na_V1.7$ channels

Considering that sibanin selectively inhibits $Na_V1.7$ channel, we sought to understand the molecular interactions between sibanin and $Na_V1.7$. Given that the application of sibanin significantly altered the voltage sensitivity of $Na_V1.7$ channels, a hallmark of a "gating modifier", we hypothesize that sibanin primarily acts on the voltage-sensor domain of the $Na_V1.7$ channel (Fig. 5a). Since $Na_V1.8$ channel is almost insensitive to sibanin, sequence alignment within the voltage-sensor domain (S3b–S4a) was constructed between the $Na_V1.7$ and $Na_V1.8$ channels (Fig. 5b). We made point mutations to the residues located on the extracellular helix-turn-helix motif region, as well as the extracellular S3–S4 linker of the $Na_V1.7$ channel (Fig. 5c). Functional screening of the mutants for the S3b–S4a identified N209 located in the S3-S4 linker of Domain I, and A1585 located in the S3–S4 linker of Domain IV as key residues for the sibanin-induced channel inhibition (Fig. 5d, e). Homologous substitution of the amino acids at the corresponding positions in the $Na_V1.8$ channel into the $Na_V1.7$ channel significantly reduced the affinity of sibanin (Fig. 5f).

To further explore the mechanism underlying the inhibitory effect of sibanin on $Na_V1.7$, we examined the voltage sensitivity and tetrodotoxin (TTX) sensitivity of $Na_V1.7$ channel mutants. Specifically, we focused on the point mutants Nav1.7-N209G and Nav1.7-A1585S, which are located in the

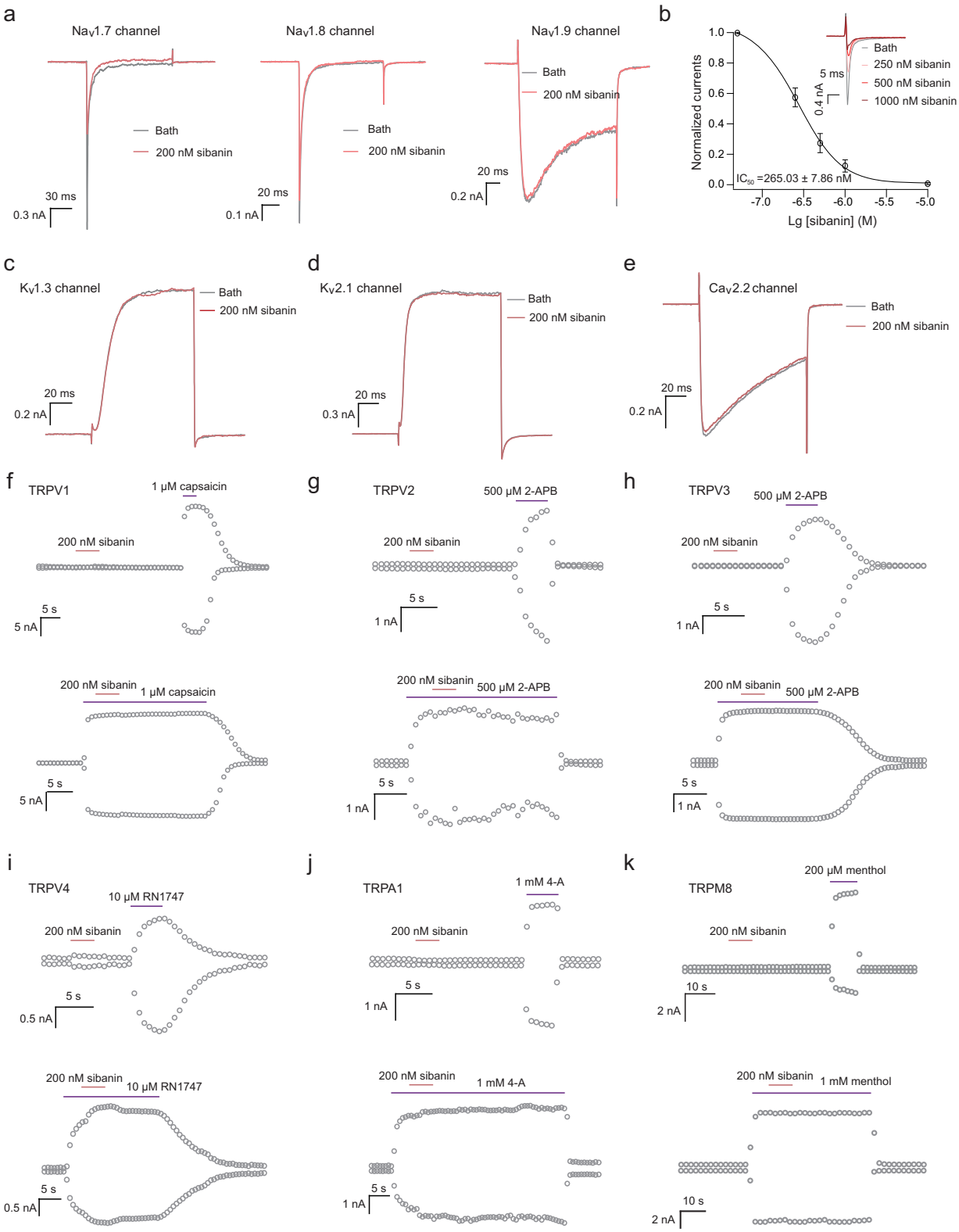

S3b–S4a region of the channel. Our results showed that neither the voltage dependence nor the TTX sensitivity of the $Na_V1.7$ channel was altered by the N209G or A1585S mutations (Fig. 5g, h). These findings suggest that the S3b-S4a region, particularly the residues N209 and A1585, is a critical site for the inhibitory action of sibanin on $Na_V1.7$. Consistent with this interpretation, the docking model of sibanin with the $Na_V1.7$ structure predicted by AlphaFold also suggests that sibanin directly interacts with the voltage-sensing domain (VSD) of the $Na_V1.7$ channel. This further supports the notion that sibanin binds to the voltage-sensing element of $Na_V1.7$, thereby inhibiting the channel function.

Fig. 3 | Sibanin selectively inhibits $Na_V1.7$ channels. a Representative current traces of human $Na_V1.7$ (left), rat $Na_V1.8$ (middle), and mouse $Na_V1.9$ (right) channels recorded in HEK293T cells under control conditions (Bath) and after 200 nM sibanin application. The $hNa_V1.7$ and $rNa_V1.8$ channels were activated by a 100-ms depolarization of −10 mV from the holding potential of −80 mV. The $hNa_V1.9$ channel was activated by a 100-ms depolarization of −40 mV from the holding potential of −120 mV. **b** (Inset) Representative $Na_V1.7$ channel current traces. The $hNa_V1.7$ channel was activated by a 100-ms depolarization of −10 mV from the holding potential of −80 mV. Dose-response curve for sibanin inhibition of $Na_V1.7$, yielding an IC_{50} of 265.03 ± 7.86 nM. Normalized currents are plotted against Log_{10}[sibanin]. **c–e** Sibanin (200 nM) application on voltage-gated potassium ($K_V1.3$, $K_V2.1$) and calcium ($Ca_V2.2$) channels. **f** TRPV1 currents activated by 200 nM sibanin (red bar, up), 1 μM capsaicin (purple bar, up), or 1 μM capsaicin in the presence of 200 nM sibanin (red bar, down). Currents were elicited by voltage ramps (−80 to +80 mV, 500 ms) at room temperature. **g** Representative TRPV2 currents activated by 200 nM sibanin (red bar, up), 500 μM 2-APB (purple bar, up), or 500 μM 2-APB in the presence of 200 nM sibanin (red bar, down). **h** Representative TRPV3 currents activated by 200 nM sibanin (red bar, up), 500 μM 2-APB (purple bar, up), or 500 μM 2-APB in the presence of 200 nM sibanin (red bar, down). **i** Representative TRPV4 currents activated by 200 nM sibanin (red bar, up), 10 μM RN1747 (purple bar, up), or 10 μM RN1747 in the presence of 200 nM sibanin (red bar, down). **j** Representative TRPA1 currents activated by 200 nM sibanin (red bar, up), 1 mM 4-A (purple bar, up), or 1 mM 4-A in the presence of 200 nM sibanin (red bar, down). **k** Representative TRPM8 currents activated by 200 nM sibanin (red bar, up), 200 μM menthol (purple bar, up), or 200 μM menthol in the presence of 200 nM sibanin (red bar, down).

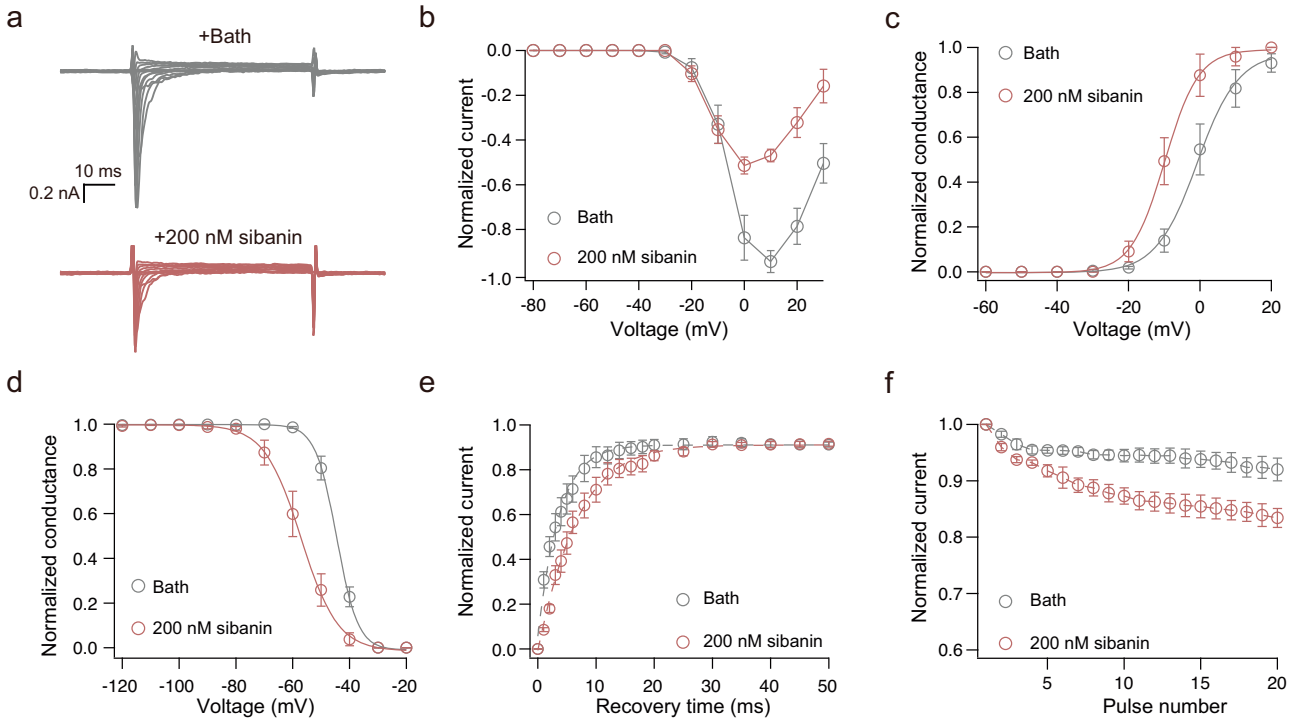

Fig. 4 | Sibanin modulates $Na_V1.7$ channel gating dynamics. a Representative current traces collected before (gray) and after perfusion (red) of 200 nM sibanin on HEK293T cell expressing $Na_V1.7$ channel. **b** Average current vs voltage relationship for the traces as in A ($n = 3$). **c** Average conductance–voltage relationship of sibanin acting on $Na_V1.7$ channel ($n = 3$). **d** Effect of 200 nM sibanin on the fast inactivation ($n = 3$). **e** Effect of sibanin on the recovery from fast inactivation. **f** Plot for sibanin inducing use-dependent inhibition. Currents were normalized to the first-pulse current in the absence (gray) or presence (red) of 200 nM sibanin and plotted against the pulse number ($n = 3$). Data were expressed as mean ± SEM.

Molecular docking of sibanin with $Na_V1.7$ channel

To resolve the structural determinants of sibanin's channel modulation, we implemented ensemble docking strategies using the $Na_V1.7$ voltage-sensing module (VSM) and sibanin's energy-minimized conformation (Fig. 5i, j). The predicted binding model revealed that sibanin adopts a β-sheet-rich conformation stabilized by three intramolecular disulfide bonds, a hallmark of Kunitz-type peptides. The C-terminal region of sibanin, enriched with basic residues, directly engages with the extracellular loops of $Na_V1.7$'s Domain I VSD (Fig. 5i). Notably, Arg16 in sibanin forms a hydrogen bond with Asn209 in the S3-S4 linker of $Na_V1.7$ (Fig. 5j), a residue critical for channel inhibition (Fig. 5e). Substitution of Asn209 with glycine (N209G) disrupted this interaction, reducing sibanin's inhibitory efficacy by 72.3 ± 5.1% ($p < 0.001$), consistent with its role as a gating modifier (Fig. 5f).

Conservation of sibanin and $Na_V1.7$ in hematophagous adaptation

Sequence alignment of sibanin with other black fly-derived Kunitz peptides (Simukunin, Guianensin, SKP1) highlighted conserved cysteine frameworks (Fig. 6a), essential for maintaining structural stability. Moreover, sibanin and its homologs harbor a conserved arginine residue in their N-terminal loop (Fig. 6a, red arrow), predicted to form a critical salt bridge with $Na_V1.7$ residue N209. Electrostatic potential maps further associate sibanin with homologs: its pronounced basic surface (Fig. 6a, blue), anchored by Arg16, is similar to the positive charge distribution observed in Simukunin and other homologs, likely enhancing their affinity for the VSD of $Na_V1.7$. The evolutionary conservation of $Na_V1.7$ residues targeted by sibanin (e.g., N209, Fig. 6b; A1585, Supplementary Fig. 4) underscores a critical adaptation strategy. By targeting a universally conserved site in vertebrate hosts, through this specific binding interaction, black flies ensure that sibanin effectively suppresses nociception across species, minimizing host detection during feeding.

The synergy between sibanin's analgesic and anticoagulant activities exemplifies a multifunctional evolutionary strategy (Fig. 6c). In cutaneous sensory neurons, sibanin binding to $Na_V1.7$ blocks action potential propagation (Fig. 2c, d), reducing nociceptive signaling to the central nervous

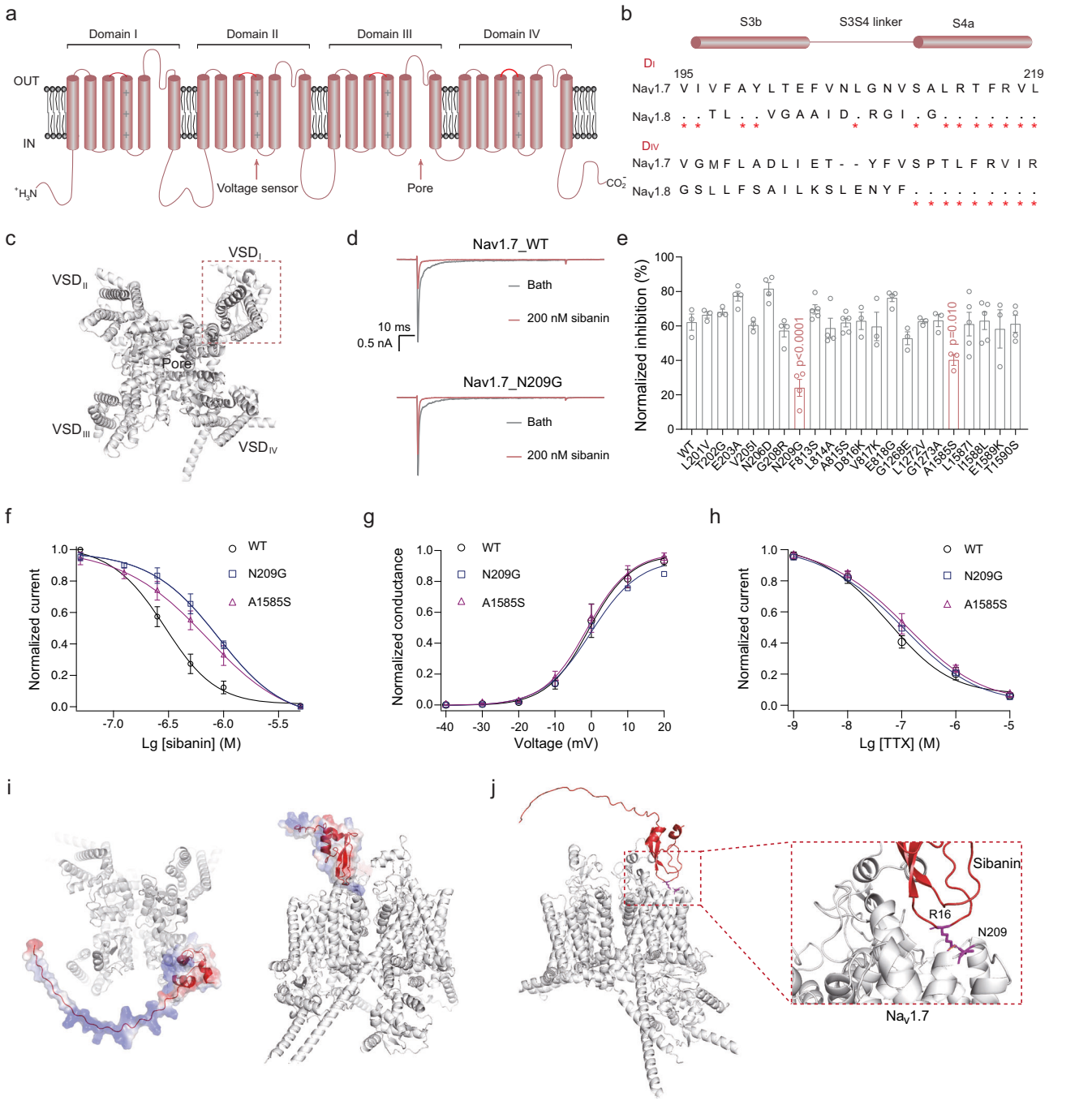

Fig. 5 | Molecular basis of sibanin binding to the $Na_V1.7$ channel. a Topological model of Nav1.7 α-subunit, highlighting four homologous domains (I–IV) with voltage-sensing modules (S1–S4) and pore-forming regions (S5–S6). **b** Zoomed view of Domain I and Domain IV voltage-sensing domain (VSD), showing critical residues in the S3b-S4 linker (e.g., N209, A1585) implicated in sibanin interaction. D_I, Domain I. D_{IV}, Domain IV. Amino acid numbering refers to the human $Na_V1.7$ channel. **c** Schematic diagram of the human $Na_V1.7$ channel structure simulated by AlphaFold3. The red dashed-line box represents the VSD I. **d** Representative current traces of $Na_V1.7$-WT and N209G mutant under control (gray) and 200 nM sibanin conditions (red). **e** The bar representing normalized inhibition currents (in %) of $Na_V1.7$ and a subset of pore region mutants in the presence of 200 nM sibanin. As compared with WT ($n = 3$-4, one-way ANOVA followed by Bonferroni's post hoc test). **f** Dose-response curves for sibanin inhibition of WT and mutant channels (N209G and A1585S). $n = 4$ for N209G; $n = 3$ for A1585S. **g** Voltage-dependent activation curves of WT and mutant $Na_V1.7$ channels. The voltage–current relationships were fitted using the Boltzmann equation to characterize gating properties. $n = 3$. **h** TTX-sensitivity curves of WT and mutant $Na_V1.7$ channels. The concentration–effect relationships were analyzed by fitting with the Hill equation. $n = 3$. **i, j** Molecular docking results of sibanin (cyan) bound to the Domain I voltage-sensing module (gray surface), highlighting key interactions with residues R16 and N209 (stick models).

system (CNS). Simultaneously, its Kunitz domain inhibits coagulation cascades, achieving dual-pathway suppression of host defenses. This dual-action mechanism not only optimizes blood-feeding efficiency but also positions sibanin as a promising lead compound for dual-target therapeutics.

Discussion

Black flies (Simuliidae) are significant hematophagous insects whose saliva contains a variety of bioactive peptides crucial for anticoagulation, antibacterial, and immunomodulatory functions[10,23]. For instance, Simukunin proteins in black fly saliva inhibit blood coagulation and inflammatory

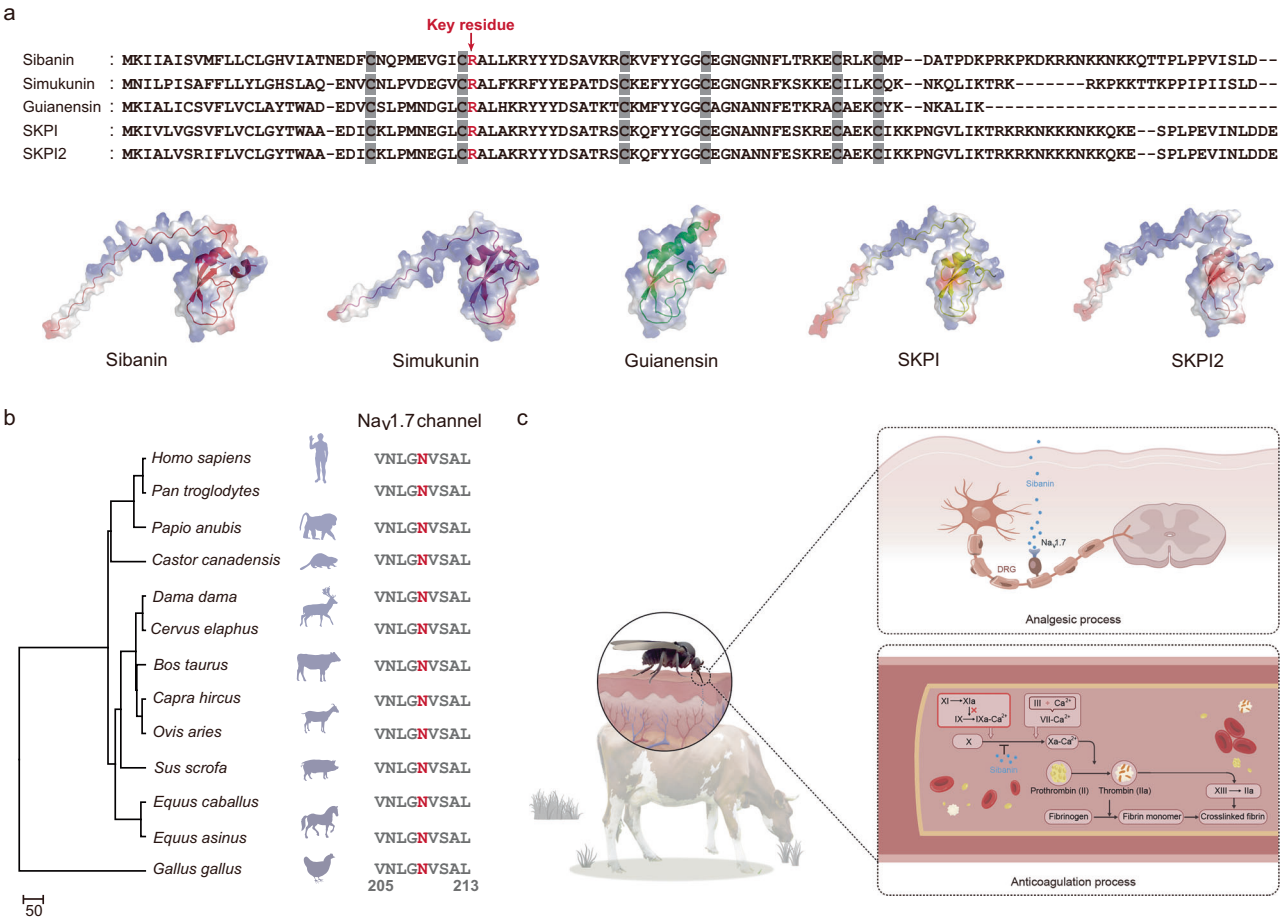

Fig. 6 | Conservation of the binding site between sibanin and the $Na_V1.7$ channel. **a** Multiple sequence alignment of sibanin and related peptides (Simukunin, Guianensin, SKPI, and SKPI2), highlighting conserved cysteine residues (gray) and functional motifs (e.g., R, red arrow). Dashes indicate sequence gaps. Electrostatic potential surface maps illustrating charge distribution (red: negative; blue: positive) of Sibanin and homologs (Simukunin, Guianensin). Ribbon diagrams depicting conserved secondary structures (α-helices: cyan; β-sheets: magenta). **b** Cross-species conservation analysis of the key residue (N209) in the $Na_V1.7$ channel, demonstrating >100% sequence identity. Species include mammalian and avian orthologs. Amino acid numbering refers to the human $Na_V1.7$ channel. **c** Molecular strategy underlying black fly predation efficiency mediated by salivary Sibanin. Sibanin potently inhibits $Na_V1.7$ voltage-gated sodium channels in peripheral sensory neurons (e.g., dorsal root ganglia), inducing localized anesthesia through blockade of action potential propagation. This suppresses nociceptive signaling to the central nervous system, effectively preventing prey awareness of feeding activity. Simultaneously, Sibanin disrupts coagulation cascades by antagonizing thrombin-mediated fibrin formation and platelet aggregation (e.g., exhibiting high-affinity binding to FXa), thereby maintaining blood fluidity and prolonging feeding duration. The dual mechanism synergistically optimizes hematophagous efficiency while minimizing host defensive responses. II, Prothrombin; III, Tissue Factor; VII, Proconvertin; IX, Christmas Factor; X, Stuart-Prower Factor; XI, Plasma Thromboplastin Antecedent; XII, Hageman Factor; XIII, Fibrin-Stabilizing Factor.

responses, while sibanin exhibits prominent anticoagulant and anti-platelet aggregation properties[12,13]. Though mechanisms by which black flies enhance blood-feeding efficiency using toxins have been extensively studied, the precise mechanism behind their potent analgesic effects remains unclear. This study aimed to elucidate the molecular mechanism of analgesia in black flies by integrating pain activity tracking and functional assays to screen the crude venom of *S. bannaense*. We identified a novel Kunitz-type protease inhibitor, sibanin, which not only demonstrates robust anticoagulant activity but also exhibits potent analgesic effects in mouse thermal pain models. Further investigations revealed that sibanin exerts its analgesic effects through selective inhibition of $Na_V1.7$ channels, and the peptide directly interacts with the VSD of $Na_V1.7$. Black flies likely utilize sibanin during blood-feeding to concurrently achieve analgesia and anticoagulation, thereby enhancing their efficiency in obtaining blood. Additionally, the unique mechanism of action and dual activity of sibanin offer significant potential value for drug development.

As the first Kunitz-type $Na_V1.7$ channel inhibitor derived from a black fly, sibanin primarily inhibits the channel through direct interaction with the VSD (S3b–S4a region). Site-directed mutagenesis experiments have revealed that residues N209 and A1585 in the $Na_V1.7$ channel are critical sites for sibanin inhibition, and mutations at both residues significantly reduce the affinity of sibanin for the $Na_V1.7$ channel. Additionally, sibanin significantly alters the voltage-dependent activation and steady-state inactivation curves of $Na_V1.7$, and substantially prolongs the recovery time of the channel from the inactivated state, indicating its mechanism as a "gating modifier". Notably, both N209 and A1585 are highly conserved among the $Na_V1.7$ channels of black fly hosts, suggesting that sibanin may exert similar analgesic effects across multiple hosts through this conserved mechanism, thereby facilitating the black fly's adaptation to its ecological niche. Notably, although A1585 exhibits evolutionary conservation equivalent to N209, its location in domain IV and the absence of direct ligand contact in our docking model suggest its influence on binding occurs through an indirect or allosteric mechanism rather than direct interaction with sibanin. Our sequence alignment across all human Na_V channels reveals that the N209 residue is conserved in $Na_V1.1$–$Na_V1.7$ and $Na_V1.9$, but is uniquely substituted in $Na_V1.8$ (Supplementary Fig. 5).

Sibanin, as a typical Kunitz-type serine protease inhibitor, exhibits potent inhibitory effects on multiple coagulation factors and proteases, including factor Xa, elastase, and cathepsin G, thereby effectively preventing thrombus formation and blood coagulation[13]. Additionally, sibanin exerts

analgesic effects by selectively inhibiting the $Na_V1.7$ channel, reducing the host's pain perception during blood-feeding and thereby minimizing the host's defensive responses. The dual activity of sibanin, combining analgesic and anticoagulant properties, significantly enhances the blood-feeding efficiency of black flies: the analgesic effect makes the host less likely to detect the blood-feeding behavior, while the anticoagulant effect ensures continuous blood flow, facilitating the efficient acquisition of blood by the flies. The structural Kunitz domain characteristic of sibanin, coupled with its multifunctional synergistic properties, renders it a uniquely evolved and highly adaptable toxin among animal venoms, with significant potential for practical applications. It is plausible that additional constituents within the extract contribute to the observed analgesic effect. The potential presence of these synergistic or independently active compounds warrants further investigation.

Sibanin also demonstrates significant clinical application potential, particularly in the management of pain and the comprehensive treatment of thrombotic diseases. By selectively inhibiting the $Na_V1.7$ channel, sibanin can precisely block pain signal transmission, thereby reducing the risk of off-target effects. The synergistic action of its anticoagulant and analgesic functions could minimize the need for combination therapy with analgesics and anticoagulants in postoperative thrombosis prevention, thereby reducing the risk of drug interactions. Furthermore, thrombosis is closely associated with chronic inflammatory conditions such as rheumatoid arthritis and diabetes, and sibanin's dual activities may potentially intervene in the pathogenesis of these diseases. Through structural optimization, evaluation of its feasibility in other disease models, and clinical trials, sibanin holds promise for the development of a new class of drugs targeting $Na_V1.7$ and coagulation pathways, addressing unmet medical needs in pain and thrombotic disease management.

Methods

Animals and ethical statement

C57BL/6 mice (8–12 weeks old, 20–25 g body weight) were procured from Vital River Laboratory Animal Technology Co., Ltd. (Beijing, China). The subjects were housed in specific pathogen-free (SPF) facilities with rigorously controlled environmental conditions: temperature maintained at 25 ± 3 °C, humidity at 60 ± 5%, and standardized photoperiod regulation (12 h light/dark cycle). Throughout the investigation, rodents received continuous access to sterilized feed and ultrapure water. All experimental procedures complied with international standards for laboratory animal care and were ethically endorsed by the Institutional Animal Care Committee of Kunming Medical University (approval ID: KMMUD20242020).

Salivary gland dissection and processing in black flies

Adult black flies were anesthetized on ice until immobile prior to dissection. Individual specimens were positioned on glass slides with a minimal volume of physiological saline (0.9% NaCl) to maintain tissue hydration. Under 40× magnification using a stereomicroscope (Leica M205C), specimens were immobilized with entomological pins at the cephalothoracic junction to expose the salivary gland complex. The glandular structures (characterized by paired translucent tubules) were carefully isolated through sequential microdissection: (1) Stabilization of the head capsule using fine-tipped forceps (Dumont #5); (2) Precise separation of salivary ducts from adjacent tissues using microdissection forceps (BioPoint MX-4); and (3) Complete extraction of intact glands through gentle traction. Immediately following dissection, salivary glands were transferred to pre-chilled microcentrifuge tubes containing ice-cold phosphate-buffered saline (PBS, pH 7.4) supplemented with protease inhibitor cocktail (Roche cOmplete™, 1:100 dilution). Samples were flash-frozen in liquid nitrogen and stored at −80 °C until processing. For protein extraction, frozen glands were subjected to ultrasonic homogenization (Sonics VCX-750, 20% amplitude) using three cycles of 10-s pulses at 20 kHz, with intermittent cooling on ice. The homogenate was centrifuged at 10,000×*g* for 15 min at 4 °C (Eppendorf 5424 R), followed by collection of the clarified supernatant for downstream analyses.

HPLC purification and N-terminal sequencing

Black fly homogenates were consolidated and subjected to lyophilization in a Labconco FreeZone 2.5 lyophilizer (−50 °C, 0.05 mbar). Chromatographic separation was conducted on a Waters HPLC system with an XBridge C18 reversed-phase column (25 cm × 4.6 mm, 5 μm particle size, 100 Å pore size) and diode array detection. A binary gradient elution method was optimized using the following phases: Phase A: 0.1% (*v*/*v*) trifluoroacetic acid (TFA, Sigma-Aldrich, ≥99.0%) in Milli-Q water (18.2 MΩ·cm); Phase B: 0.1% (*v*/*v*) TFA in HPLC-grade acetonitrile (Honeywell). The separation protocol comprised a 70-min linear gradient from 20% to 80% Phase B at 1.0 mL/min, with simultaneous UV absorbance monitoring at 215 nm (peptide bonds) and 280 nm (aromatic residues). Target fractions were isolated and concentrated via vacuum evaporation.

For N-terminal sequence analysis, purified peptide samples (100 pmol/μL in 0.1% formic acid) underwent Edman degradation using an Applied Biosystems Procise 491 pulsed-liquid phase sequencer. The procedure was carried out according to the manufacturer's protocols to ensure accurate determination of the amino acid sequence. Automated cycles (20 cycles) were performed with phenylisothiocyanate (PTC) coupling in 20% (*v*/*v*) trimethylamine, followed by cleavage with anhydrous TFA. Resultant phenylthiohydantoin (PTH) derivatives were analyzed by online HPLC using the manufacturer's standard PTH analyzer module. Sequence data were processed using Protein Sequencer Data Analysis Software v2.1 (Thermo Fisher Scientific).

Heterologous expression and purification of recombinant sibanin

The sibanin coding sequence was determined through sequencing and BLAST alignment analysis. For prokaryotic expression, the cDNA was synthesized with *KpnI* and *HindIII* restriction sites flanking the 5'- and 3'-termini, respectively, to facilitate directional cloning. A tobacco etch virus (TEV) protease recognition site was incorporated immediately downstream of the 5' KpnI site to enable subsequent cleavage of the fusion protein. The entire sequence was codon-optimized for *Escherichia coli* expression. The optimized gene was cloned into the pET-32a(+) expression vector (Novagen) using the engineered restriction sites, creating an in-frame fusion to the C-terminus of the thioredoxin (Trx) tag to enhance protein solubility. The vector's inherent N-terminal hexahistidine (His_6) tag facilitated affinity purification. The recombinant plasmid was transformed into *E. coli* Rosetta(DE3) competent cells. Protein expression was induced with 0.5 mM isopropyl β-D-1-thiogalactopyranoside (IPTG), and production was verified by SDS-PAGE. The His_6-Trx-sibanin fusion protein was purified under denaturing conditions using Ni-NTA affinity chromatography. The fusion partner was cleaved by TEV protease incubation (1:50 *w*/*w*, 16 °C, 16 h), followed by reverse-phase HPLC purification on a C4 XBridge BEH column (10 × 250 mm) to isolate native sibanin and remove salts.

Thermal nociception assessment using the hot-plate test

The hot-plate pain meter (ZS-CTE) was calibrated to 52.0 ± 0.5 °C for standardized thermal stimulation. Female C57BL/6 mice (20–25 g, 10–12 weeks) were acclimatized to the testing environment for 30 min prior to baseline measurements. Each group of six mice was housed in a single cage. Confounders were not controlled. Mice underwent primary screening at 50 °C to exclude hypersensitive (<5 s) or non-responsive (>30 s) individuals based on nociceptive latency (hind paw licking/jumping). Mice were randomized into five groups ($n = 6$ / group): saline control, three polypeptide-treated groups (0.2, 1.0, 5.0 mg/kg), and morphine (0.2 mg/kg). Baseline latency was determined through triplicate measurements (10-min intervals), followed by intraperitoneal injection and post-treatment assessments at 30 min–16 h with a 60-s cutoff. Analgesic efficacy (%) was calculated relative to baseline, with data analyzed via Student's *t*-test (vs control) and one-way ANOVA (inter-group) using SPSS v26, presented as mean ± SEM. Experimenters were blinded to treatment groups, independently coded solutions, and decoded post-analysis. The protocol emphasized

standardized equipment, rigorous screening, and quantitative pharmacological evaluation. The subjects, investigators, and data analysts are all blinded.

Paclitaxel-induced neuropathic pain

Neuropathic pain was induced in mice (C57BL/6 mice, both sexes, 20–25 g, 8–12 weeks) through four intraperitoneal injections of paclitaxel (4 mg/kg per dose) administered at 48-h intervals. Each group of six mice was housed in a single cage. Confounders were not controlled. Mechanical allodynia was quantified 10-12 days post-initial treatment using von Frey filaments via the up-down paradigm. The chemotherapeutic agent was prepared in a vehicle solution containing 17% Cremophor EL, 17% ethanol, and 66% saline (*v*/*v*). During the assessment, responses to mechanical stimuli were recorded meticulously. A positive response, defined as withdrawal of the tested paw, was marked as "X" while a negative response (no withdrawal) was noted as "0". The mechanical threshold for 50% withdrawal probability was calculated using the formula:

$$50\%\ \text{threshold (g)} = (10^{(\text{Xf}+\kappa\cdot\partial)})/10,000$$

In this formula, X_f represents the value (in log units) of the final von Frey hair utilized in the test. The variable κ is determined according to the pattern of the recorded responses. The symbol ∂ denotes the mean difference (in log units) between stimuli. The subjects, investigators, and data analysts are all blinded.

Cell culture and transfection protocol

HEK293T cells (ATCC CRL-3216) were cultured in DMEM (D6546, Thermo Fisher Scientific) containing 4.5 g/L glucose, 10% FBS (12106 C, TFS), and 1% antibiotic-antimycotic cocktail (PB180121, Procell) under standard incubator conditions (37 °C, 5% CO_2, humidified atmosphere). Subculturing was performed at 70–90% confluency using 0.25% trypsin-EDTA (TFS). For transient transfection studies, cells were plated in 35–mm Falcon culture dishes 24 h pre-transfection. Modified Lipofectamine 3000 (L3000015, TFS) transfection complexes were prepared as follows: Solution A: 6 μL Lipofectamine 3000 + 200 μL Opti-MEM (31985070, TFS); Solution B: 5 μg target plasmid + 0.5 μg pEGFP-N1 (Clontech) + 6 μL P3000 Enhancer + 200 μL Opti-MEM. After separating 5-min equilibration at ambient temperature (22–25 °C), Solutions A/B were combined with gentle vortex mixing. Following 15-min complex formation, transfection mixtures were administered dropwise to adherent cells. Electrophysiological assessments were conducted 24–36 h post-transfection.

Isolation and primary culture of DRG neurons

Oxygenated Dulbecco's Modified Eagle Medium (DMEM, Sigma-Aldrich D5648) was prepared by dissolving 346 mg DMEM powder and 74 mg $NaHCO_3$ in 20 mL ultrapure water (Milli-Q, 18.2 MΩ), followed by sterile filtration (0.22 μm PVDF membrane) and equilibration with carbogen gas (95% O_2/5% CO_2) for 15 min using a gas-perfusion system (Harvard Apparatus). Enzymatic digestion solution containing 1.0 mg/mL trypsin (T1426, Sigma-Aldrich) and 2.2 mg/mL collagenase type I (C0130, Sigma-Aldrich) was prepared in oxygenated DMEM, while 1.2 mg/mL soybean trypsin inhibitor (T9128, Sigma-Aldrich) in calcium-free Hank's Balanced Salt Solution served as an enzymatic termination reagent.

Adult C57BL/6 mice (25–30 g, mixed sex) were euthanized via cervical dislocation under IACUC-approved protocols. Vertebral columns were rapidly dissected and bisected sagittally in oxygenated DMEM at 4 °C. Twenty dorsal root ganglia (DRGs) from thoracic-lumbar regions were microdissected using Dumont #5 forceps under stereomicroscopic guidance (Leica M80), followed by mechanical dissociation with Vannas spring scissors (15000-03, Fine Science Tools) into <1 mm^3 fragments. Tissue fragments underwent enzymatic digestion (37 °C, 180 rpm, 25 min) in a temperature-controlled orbital shaker (Thermo Scientific MaxQ 4450), with intermittent agitation every 5 min. Digested suspensions were quenched with trypsin inhibitor, centrifuged at 300×*g* for 5 min (Eppendorf 5430R), and resuspended in serum-supplemented DMEM (10% FBS, identical to HEK293T culture conditions). Cells were plated on poly-L-lysine-coated 8 mm glass coverslips (0111520, Warner Instruments) within 35 mm culture dishes and maintained at 37 °C/5% CO_2 for 4 h to ensure adhesion prior to electrophysiological experiments.

Electrophysiological recordings

Whole-cell patch-clamp recordings were performed using a HEKA EPC-10 Double amplifier system (HEKA, Germany) interfaced with PatchMaster v2x90 software. Borosilicate glass capillaries (1.5 mm, Sutter Instrument BF150-86-10) were pulled using a P-97 micropipette puller (Sutter Instrument) to achieve tip resistances of 3-5 MΩ when filled with intracellular solution. These micropipettes were used to form high-resistance seals on green fluorescent HEK293T cells, followed by membrane rupture to establish a whole-cell configuration for recording sodium channel currents. After achieving whole-cell configuration, capacitive transients and leak currents were subtracted. Series resistance was compensated by 75 ± 5% and continuously monitored. Recordings were terminated if series resistance exceeded 10 MΩ or changed by >20% during the experiment. Bath solution and sibanin were delivered via a gravity-driven perfusion system (Bio-Logic, RSC-200). During recording, the cell membrane potential was clamped at −80 mV, with a stimulation voltage set at 0 mV. To record current–voltage relationships, a voltage gradient from −80 mV to +50 mV (in 10 mV steps, each lasting 100 ms) was applied to activate $Na_V1.7$ channels and record peak currents. The conductance–voltage relationship was fitted using the Boltzmann equation for accurate electrophysiological characterization of $Na_V1.7$ channels. The pipette solution contained (in mM): 144 KCl, 7.6 $CaCl_2$, 1.2 $MgCl_2$, 10 EGTA, and 10 HEPES (pH 7.2 with KOH). The bath solution contained (in mM): 140 NaCl, 4 KCl, 0.1 $CaCl_2$, 3 $MgCl_2$, and 10 HEPES (pH 7.4 with KOH). Moreover, the $Na_V1.8$ and $Na_V1.9$ plasmids were transfected into ND7/23 cells. 1 μM TTX was used to inhibit the TTX-sensitive (TTX-S) current in ND7/23 cells. The EC_{50} value was calculated by fitting data points using the Hill equation:

$$I/I_{\max} = 1/[1 + (EC_{50}/[D])^{n_H}]$$

Currents were sampled at 50 kHz with 10 kHz Bessel filtering. Voltage-dependent activation curves were fitted with the Boltzmann equation:

$$G/G_{\max} = 1/[1 + exp((V_{1/2} - V_m)/k$$

where $V_{1/2}$ = half-activation voltage, k = slope factor.

Similar protocols were applied for functional characterization of $Na_V1.8$, $Na_V1.9$, TRPV1-4, TRPA1, $K_V1.3$, and $K_V2.1$ channels with channel-specific modifications: For the $Na_V1.8$ channel, internal (mM): 140 CsCl, 10 NaCl, 1 EGTA, 20 HEPES, 2 Mg-ATP (pH 7.3 with CsOH). External (mM): 140 NaCl, 2 $CaCl_2$, 1 $MgCl_2$, 5 KCl, 20 mM HEPES, 10 glucose (pH 7.4 with NaOH). Protocol: −80 mV holding; −10 mV test pulses (100 ms). For $Na_V1.9$ channel, internal (mM): 105 CsF, 35 NaCl, 10 EGTA, 10 HEPES (pH 7.3 with CsOH). External (mM): 150 NaCl, 1.5 $CaCl_2$, 1 $MgCl_2$, 2 KCl, 10 mM HEPES (pH 7.4 with NaOH). Protocol: −120 mV holding; −40 mV test pulses (100 ms). For TRP channel, both internal and external (mM): 130 NaCl, 0.2 EDTA, 3 HEPES (pH 7.2 with HCl). For $K_V1.3$ channel, internal (mM): 140 KCl, 1 $CaCl_2$, 2 $MgCl_2$, 10 EGTA, 10 HEPES (pH 7.3 with KOH). External (mM): 150 NaCl, 0.5 $CaCl_2$, 1.2 $MgCl_2$, 5 KCl, 10 HEPES (pH 7.3 with NaOH). Protocol: -80 mV holding; 0 mV test pulses (100 ms). For the $K_V2.1$ channel, internal (mM): 140 KCl, 1 Mg-ATP, 1 $MgCl_2$, 5 EGTA, 10 HEPES (pH 7.25 with KOH). External (mM): 137 NaCl, 1.8 $CaCl_2$, 1 $MgCl_2$, 5.4 KCl, 10 Glucose (pH 7.4 with NaOH). Protocol: −80 mV holding; 0 mV test pulses (100 ms). Human $Na_V1.9$ was expressed in ND7/23 cells following established protocols[24]. Transfections employed X-tremeGENE HP DNA Transfection Reagent (Roche) per manufacturer specifications: 4 μg $hNa_V1.9$-GFP plasmid complexed with 8 μL reagent. Post-transfection, cells underwent sequential incubation: 24 h at 37 °C/5% CO_2 followed by 20 h at 29 °C/5%

CO_2 prior to electrophysiological recording. GFP fluorescence facilitated visual identification of successfully transfected cells.

Voltage-clamp recordings from mouse DRGs were performed with the following solutions: for K_V channel recordings, intracellular solution contained 140 mM KCl, 10 mM HEPES, 10 mM EGTA, and 4 mM Mg-ATP (pH 7.2 adjusted with 1 M KOH), with extracellular solution comprising 5.4 mM KCl, 135 mM NaCl, 1 mM $MgCl_2$, 0.33 mM NaH_2PO_4, 10 mM HEPES, and 10 mM glucose (pH 7.4 adjusted with 1 M NaOH); for Na_V channels, intracellular solution used 10 mM NaCl, 5 mM HEPES, and 135 mM CsF (pH 7.2 with 1 M CsOH), while extracellular solution contained 30 mM NaCl, 1.8 mM $CaCl_2$, 1 mM $MgCl_2$, 5 mM CsCl, 5 mM HEPES, 90 mM TEA-Cl, and 25 mM glucose (pH 7.4 adjusted with 1 M TMAH); for Ca_V channels, intracellular solution consisted of 110 mM CsCl, 5 mM $MgSO_4$, 25 mM HEPES, 10 mM EGTA, and 2 mM ATP (pH 7.2 with 1 M CsOH), with extracellular solution containing 125 mM TEA-Cl, 10 mM $BaCl_2$, 5 mM HEPES, and 5 mM glucose (pH 7.2 adjusted with 1 M TMAH). To record the membrane excitability of DRG neurons from mice, the extracellular solution consisted of: 140 mM NaCl, 3 mM KCl, 2 mM $CaCl_2$, 2 mM $MgCl_2$, 10 mM HEPES (pH 7.3 with NaOH), and the intracellular solution contained: 140 mM KCl, 0.5 mM EGTA, 10 mM HEPES, and 2 mM Mg-ATP (pH 7.3 with KOH). Action potentials were recorded from DRG neurons paced at 1 Hz. Data were acquired using PatchMaster software (HEKA, Germany) and digitized at 1 kHz. Data analysis was done using Igor Pro (Wavemetrics, Portland, OR) and Prism (Graphpad, La Jolla, CA). The recordings were acquired in a current-clamp mode, and parameters related to AP firing, including resting membrane potential (RMP), amplitude, and firing frequency, were determined.

Construction of $Na_V1.7$ channel mutants

The point mutants of $Na_V1.7$ were prepared using the QuikChange Lightning Site-Directed Mutagenesis Kit (Agilent 210518). The specific steps are as follows. To introduce single-base site-directed mutations into the plasmid, a pair of PCR primers was designed to introduce the mutations. The principles for primer design were as follows: The 5' ends of the forward and reverse amplification primers contained a 21–25 bp reverse-complementary region. The length of the non-complementary region of each primer was at least 15 bp, and the introduced mutation site was within the complementary region of the two primers. The PCR reaction system was composed as follows: 5 μL of 10× reaction buffer, 10 ng of dsDNA template, 125 ng of oligonucleotide forward primer, 125 ng of oligonucleotide reverse primer, 1 μL of dNTP mix, 1.5 μL of QuikSolution reagent, and ddH_2O was added to a final volume of 50 μL. Finally, 1 μL of QuikChange Lightning Enzyme was added. The PCR reaction program was set as: 95 °C for 5 min (1 cycle), followed by 30 cycles of 95 °C for 20 s, 60 °C for 10 s, and 68 °C for 30–60 s/kb, and then 68 °C for 5 min (1 cycle). Two μL of the restriction enzyme Dpn I was added, and the mixture was digested at 37 °C for 15 min to completely remove the methylated template plasmid in the reaction mixture, preventing the formation of false-positive transformant clones in subsequent experiments. The digested reaction products were transformed into XL10-Gold super-competent cells. The transformed products were centrifuged at 1000 rpm for 3 min. The supernatant was discarded, and the bacterial pellet was resuspended in 100 μL of freshly prepared liquid LB medium (without antibiotics). The suspension was evenly spread on a 60-mm LB solid plate (containing the appropriate type of antibiotic). After incubation at 37 °C for 24 h, the grown clones were sequenced for verification.

Molecular docking

The amino-acid sequence of sibanin (UniProt ID: 1NIX) was obtained from the UniProt database. The three-dimensional structure of the $Na_V1.7$ channel was predicted and constructed using AlphaFold 2. The resulting $Na_V1.7$ channel model was imported into the Discovery Studio 2019 software for energy minimization and structural refinement to enhance its precision. Molecular docking between sibanin and the $Na_V1.7$ channel (PDB ID: 6CNM) was executed using ZDOCK with the following parameters: angular increment of 6°, RMSD threshold of 6.0, interface distance cutoff of 9.0, and a maximum of 60 clusters. Following the docking process, the highest-scoring conformation based on the ZDOCK scoring algorithm was selected. Subsequently, the conformation with the lowest energy was identified using the E_RDOCK scoring metric.

Blood coagulation time analyses

To evaluate the anticoagulant properties of sibanin across coagulation pathways, both activated partial thromboplastin time (aPTT) and prothrombin time (PT) were determined. For aPTT and PT analyses, distinct procedures were implemented: PT measurement involved 3-min incubation of 40 μL plasma with 10 μL sibanin (12.5–50 nM) and 50 μL PT reagent (Leagene, China) at 37 °C prior to immediate coagulation time recording; aPTT determination required initial 3-min incubation of the plasma–sibanin mixture with 50 μL aPTT reagent (Beyotime, China) at 37 °C, followed by $CaCl_2$-triggered clotting. Both assays employed identical optical detection parameters to ensure methodological consistency.

Serine protease inhibition assays

The enzymatic modulation of sibanin on serine proteases (factor Xa, plasma kallikrein, elastase, trypsin) was investigated through chromogenic substrate hydrolysis assays under standardized conditions (50 mM Tris-HCl, pH 7.8, 150 mM NaCl, 37 °C). Following 10-min pre-treatment of individual proteases with 1000 nM sibanin or vehicle control, enzymatic reactions were triggered by introducing specific chromogenic substrates (final concentration 0.5 mM) into the reaction system. Real-time hydrolysis kinetics were captured by monitoring p-nitroaniline release through continuous absorbance measurement at 405 nm using a full-wavelength microplate reader (Thermo Fisher Scientific, USA), with baseline correction performed against blank controls containing substrate alone. This configuration enabled precise quantification of Sibanin-induced enzymatic activity changes through comparative analysis of reaction slopes between treatment groups.

Statistics and reproducibility

All quantitative data are expressed as mean ± standard error of mean (SEM). Statistical analyses were performed using a dual-platform approach. Behavioral and biochemical data were analyzed in GraphPad Prism 9.0 with Student's *t*-test for pairwise comparisons, One-way ANOVA with Bonferroni post-hoc correction for multi-group analyses. Electrophysiological parameters were processed using Igor Pro 6.0 (WaveMatrix) with custom-developed protocols, automated curve fitting using built-in Boltzmann equation, Hill equation for dose–response relationships, and channel recovery kinetics analyzed with single exponential functions. Molecular docking results were validated through Root-mean-square deviation (RMSD) cluster analysis, binding energy calculations using the CHARMM force field, and Electrostatic potential surface mapping in Discovery Studio 2019. Statistical significance thresholds were set at $P < 0.05$ (single asterisk), $^{*}p < 0.01$ (double asterisk), and $^{**}p < 0.001$ (triple asterisk). All Figures were generated using GraphPad Prism 9.0 with consistent formatting.

Reporting summary

Further information on research design is available in the Nature Portfolio Reporting Summary linked to this article.

Data availability

The data that support this study are available from the corresponding authors upon reasonable request. All data are contained within the article and supplementary information files. The source data underlying Figs.1c, 2a, b, d–f, h, 3b, 4b–f, and 5e–h and Supplementary Figs. 1a,–3 are provided as the Source Data Files. The Source Data file (Supplementary Data 1) is included in the supplementary information.

Received: 30 April 2025; Accepted: 5 November 2025;
Published online: 23 November 2025

References

1. Luo, L. et al. Centipedes subdue giant prey by blocking KCNQ channels. *Proc. Natl. Acad. Sci. USA* **115**, 1646–1651 (2018).
2. Yang, S. et al. A bimodal activation mechanism underlies scorpion toxin–induced pain. *Sci. Adv.* **3**, e1700810 (2017).
3. Ligabue-Braun R. Venom use in mammals: evolutionary aspects. *Evolution of Venomous Animals and Their Toxins* 235–257 (Springer, Dordrecht, 2017).
4. Fischer, T. & Riedl, R. Paracelsus' legacy in the faunal realm: drugs deriving from animal toxins. *Drug Discov. today* **27**, 567–575 (2022).
5. Jin, L. et al. Salivary factor LTRIN from *Aedes aegypti* facilitates the transmission of Zika virus by interfering with the lymphotoxin-β receptor. *Nat. Immunol.* **19**, 342–353 (2018).
6. Wang, C. et al. Isolation and characterization of poeciguamerin, a peptide with dual analgesic and anti-thrombotic activity from the Poecilobdella manillensis leech. *Int. J. Mol. Sci.* **24**, 11097 (2023).
7. Shakouri, A. & Wollina, U. Time to change theory; medical leech from a molecular medicine perspective leech salivary proteins playing a potential role in medicine. *Adv. Pharm. Bull.* **11**, 261 (2020).
8. Zheng, J. et al. Molecular mechanisms underlying hematophagia revealed by comparative analyses of leech genomes. *Gigascience* **12**, giad023 (2023).
9. Mullen G. R. & Durden L. A. *Medical and Veterinary Entomology* (Academic Press, 2009).
10. Cupp, E. W. & Cupp, M. S. Black fly (Diptera: Simuliidae) salivary secretions: importance in vector competence and disease. *J. Med. Entomol.* **34**, 87–94 (1997).
11. Andersen, J. F., Pham, V. M., Meng, Z., Champagne, D. E. & Ribeiro, J. M. Insight into the sialome of the black fly, *Simulium vittatum*. *J. Proteome Res.* **8**, 1474–1488 (2009).
12. Tsujimoto, H. et al. Simukunin from the salivary glands of the black fly Simulium vittatum inhibits enzymes that regulate clotting and inflammatory responses. *PLoS One* **7**, e29964 (2012).
13. He, Y. et al. Sibanin, a novel black fly-derived Kunitz protease inhibitor, prevents thrombus formation in mice by anticoagulation-antiplatelet duality. *Int. J. Biol. Macromol.* **296**, 139766 (2025).
14. Woolf, C. J. & Ma, Q. Nociceptors—noxious stimulus detectors. *Neuron* **55**, 353–364 (2007).
15. Strickland, I. T. et al. Changes in the expression of NaV1. 7, NaV1. 8 and NaV1. 9 in a distinct population of dorsal root ganglia innervating the rat knee joint in a model of chronic inflammatory joint pain. *Eur. J. Pain* **12**, 564–572 (2008).
16. Bennett, D. L., Clark, A. J., Huang, J., Waxman, S. G. & Dib-Hajj, S. D. The role of voltage-gated sodium channels in pain signaling. *Physiol. Rev.* **99**, 1079–1151 (2019).
17. Hao, J. et al. Kv1. 1 channels act as mechanical brake in the senses of touch and pain. *Neuron* **77**, 899–914 (2013).
18. Wickenden, A. & McNaughton-Smith, G. Kv7 channels as targets for the treatment of pain. *Curr. Pharm. Des.* **15**, 1773–1798 (2009).
19. Winquist, R. J., Pan, J. Q. & Gribkoff, V. K. Use-dependent blockade of Cav2. 2 voltage-gated calcium channels for neuropathic pain. *Biochem. Pharmacol.* **70**, 489–499 (2005).
20. Julius, D. TRP channels and pain. *Annu. Rev. Cell Dev. Biol.* **29**, 355–384 (2013).
21. Brederson, J.-D., Kym, P. R. & Szallasi, A. Targeting TRP channels for pain relief. *Eur. J. Pharmacol.* **716**, 61–76 (2013).
22. Cortright, D. N. & Szallasi, A. TRP channels and pain. *Curr. Pharm. Des.* **15**, 1736–1749 (2009).
23. Adler, P. H. & McCreadie, J. W. Black flies (Simuliidae). In: *Medical and Veterinary Entomology* (Elsevier, 2019).
24. Zhou, X. et al. Electrophysiological and pharmacological analyses of Na1.9 voltage-gated sodium channel by establishing a heterologous expression system. *Front. Pharmacol.* **8**, 852 (2017).

Acknowledgements

This work was supported by the Chinese National Natural Science Foundation (U24A20812, 32060119, 31970418), Applied Basic Research Foundation of Yunnan Province (202501AS070024, 202301AY070001-015), the Yunnan Revitalization Talent Support Program (YUWR-QNBJ-2019-189), and First-Class Discipline Team of Kunming Medical University (2024XKTDYS02).

Author contributions

H.Y., J.W., and L.M. designed the experiments. X.Y., Y.H., and X.F. conducted the experiments. G.W. and X.Z. participated in the discussion of the results. X.Y. analyzed the data. H.Y. and X.Y. drafted the manuscript.

Competing interests

The authors declare no competing interests.

Additional information

Supplementary information The online version contains supplementary material available at https://doi.org/10.1038/s42003-025-09182-6.

Correspondence and requests for materials should be addressed to Lixian Mu, Jing Wu or Hailong Yang.

Peer review information *Communications Biology* thanks Thomas Ravenscroft, Diogo Tibery, and the other, anonymous, reviewer(s) for their contribution to the peer review of this work. Primary Handling Editors: Asuka Takeishi and Benjamin Bessieres.